

FSDPT based study for vibration analysis of piezoelectric coupled annular FGM plate[†]

Farzad Ebrahimi* and Abbas Rastgoo

Department of Mechanical Engineering, University of Tehran, Tehran, Iran

(Manuscript Received October 27, 2008; Revised December 30, 2008; Accepted March 18, 2009)

Abstract

The vibration behavior of a piezoelectrically actuated thick functionally graded (FG) annular plate is studied based on first order shear deformation plate theory (FSDPT). A consistent formulation that satisfies the Maxwell static electricity equation is presented so that the full coupling effect of the piezoelectric layer on the dynamic characteristics of the annular FG plate can be estimated based on the free vibration results. The differential equations of motion are solved analytically for various boundary conditions of the plate. The analytical solutions are derived and validated by comparing the obtained resonant frequencies of the composite plate with those of an isotropic core plate. As a special case, assuming that the material composition of core plate varies continuously in the direction of the thickness according to a power law distribution, a comprehensive study is conducted to show the influence of functionally graded index on the vibration behavior of smart structure. Also, the good agreement between the results of this paper and those of the finite element (FE) analyses validates the presented approach.

Keywords: FSDPT; Functionally graded materials; Annular plate; Free vibration

1. Introduction

The structures having built-in mechanisms for achieving self-controlling and/or self-monitoring capabilities are customarily known as 'smart structures'. The study of embedded or surface-mounted piezoelectric materials in such structures has received considerable attention in recent years because piezoelectric materials are more extensively used either as actuators or sensors. To effectively utilize the piezoelectric effect and actuating properties of piezoelectric materials, the interaction between the host structure and piezoelectric patch must be well understood. Laminated composite structures can be tailored to design advanced structures, but the sharp change in the properties of each layer at the interface between

two adjacent layers causes large inter-laminar shear stresses that may eventually give rise to the well known phenomenon of delamination. Such detrimental effects can be mitigated by grading the properties in a continuous manner across the thickness direction. Functionally graded materials (FGMs) are inhomogeneous composite materials that are made from different phases of materials such as ceramic and a metal. FGMs have different applications especially for space vehicles, defense industries, and biomedical sectors. FGM properties vary continuously from one interface to the other. Those are achieved by gradually varying volume fraction of constituent materials.

Recently, considerable interest has been focused on investigating the performance of FGM plates integrated with piezoelectric actuators. For example, Wang and Noda [1] analyzed a smart FGM composite structure composed of a layer of metal, a layer of piezoelectric and a FGM layer in between, while in [2] a finite element model was developed for studying

[†] This paper was recommended for publication in revised form by Associate Editor Eung-Soo Shin

*Corresponding author. Tel.: +91 21 8800 5677, Fax.: +98 21 8801 3029
E-mail address: febrahimi@ut.ac.ir

© KSME & Springer 2009

the shape and vibration control of FGM plates integrated with piezoelectric sensors and actuators. The post buckling behavior of rectangular FGM plate with its surface bonded to piezoelectric actuators under the combined action of thermo-electro-mechanical loadings was examined by Liew et al. [3] and by Shen [4]. Yang et al. [5] investigated the nonlinear thermo-electro-mechanical bending response of FG rectangular plates that are covered with monolithic piezoelectric actuator layers on the top and bottom surfaces of the plate. They [6] also presented a large amplitude vibration analysis of a rectangular FGM plate with surface-bonded piezoelectric layers by using a semi-analytical method based on 1D differential quadrature and Galerkin technique. Most recently, Huang and Shen [7] investigated the dynamics of an FGM plate coupled with two monolithic piezoelectric layers at its top and bottom surfaces undergoing nonlinear vibrations in thermal environments.

To the authors' best knowledge, no researches dealing with the free vibration characteristics of the circular and annular FGM plate integrated with the piezoelectric layers have been reported in literature except the author's recently published works in presenting an analytical solution for the free axisymmetric vibration of piezoelectric coupled thin and thick circular and thin annular FGM plates [8-12]. In conjunction with these works, we attempt to provide an analytical solution for free vibration of thick annular FGM plates with two full size surface-bonded piezoelectric layers on the top and the bottom of the FGM plate. The formulations are based on first order shear deformation plate theory. The differential equations of motion are solved analytically for various boundary conditions of the plate through the transformation of variable method. The applicability of the proposed model is analyzed by studying the effect of varying the gradient index of FG plate on the free vibration characteristics of the structure. For some specific cases, the obtained results were cross checked with the existing literature and furthermore, verified by those obtained from three-dimensional finite element (3D FE) analyses.

2. FG and piezoelectric materials

2.1 Functionally graded materials (FGM)

Nowadays, not only can FGM be easily produced but one can control even the variation of the FG constituents in a specific way. Several available analyti-

cal and computational models have discussed the issue of finding suitable functions for FGM's material properties. They are desired to be continuous, simple and should have the ability to exhibit curvature, both "concave upward" and "concave downward" [13]. In this study the simple power law, which has all the desired properties, is used by which, in an FG material made of ceramic and metal mixture, we have

$$V_m + V_c = 1 \quad (1)$$

in which V_c and V_m are the volume fraction of the ceramic and metallic part, respectively. Based on the power law distribution [14], the variation of V_c vs. thickness coordinate (z) with its origin placed at the middle of thickness, can be expressed as

$$V_c = (z/2h_f + 1/2)^g, \quad g \geq 0, \quad (2)$$

where z is measured from the mid-plane of the plate in the transverse direction and $2h_f$ is the FG core plate thickness and g is the FGM volume fraction index which takes values greater than or equal to zero (see Fig. 1). All other mechanical, physical and thermal properties of FGM media follow the same distribution as for V_c . We assume that the inhomogeneous material properties, such as the modulus of elasticity E and the density ρ change within the thickness direction z based on Voigt's rule over the whole range of the volume fraction as following [15]; while Poisson's ratio ν is assumed to be constant in the thickness direction as [16]

$$\begin{aligned} E(z) &= (E_c - E_m)V_c(z) + E_m \\ \rho(z) &= (\rho_c - \rho_m)V_c(z) + \rho_m \\ \nu(z) &= \nu \end{aligned} \quad (3)$$

where subscripts m and c refer to the metal and ceramic constituents, respectively. After substituting V_c from Eq. (2) into Eq. (3), material properties of the FGM plate are determined in the power law form which are the same as those proposed by Reddy and Praveen [14] i.e.

$$E(z) = (E_c - E_m)(z/2h_f + 1/2)^g + E_m \quad (4)$$

$$\rho(z) = (\rho_c - \rho_m)(z/2h_f + 1/2)^g + \rho_m \quad (5)$$

The above power law assumption reflects a simple rule of mixtures used to obtain the effective properties of the ceramic-metal plate. The rule of mixtures ap-

plies only to the thickness direction. If $g=0$, then the plate reduces to a pure ceramic plate. As the volume fraction index g increases, the ceramic volume fraction decreases and in the same z/h , by increasing g dimensionless Young's modulus decreases.

Contrary to the most of the published papers on the FG plates, in this paper we choose a plate with upper part as being metallic and the lower part as ceramic. This makes us to exchange subscript m in the Eqs (4), (5) with c and vice versa. In this way, when $g=0$ the FG plate becomes completely a metallic isotropic plate.

2.2 Piezoelectric materials

The constitutive 2D elasto-static relation for symmetry piezoelectric materials in Cartesian coordinate can be represented as [17]

$$\begin{pmatrix} \sigma_{11} \\ \sigma_{22} \\ \sigma_{12} \\ \sigma_{13} \\ \sigma_{23} \end{pmatrix} = \begin{pmatrix} \bar{C}_{11}^E & \bar{C}_{12}^E & 0 & 0 & 0 \\ \bar{C}_{12}^E & \bar{C}_{11}^E & 0 & 0 & 0 \\ 0 & 0 & (\bar{C}_{11}^E - \bar{C}_{12}^E)/2 & 0 & 0 \\ 0 & 0 & 0 & \kappa^2 C_{55}^E & 0 \\ 0 & 0 & 0 & 0 & \kappa^2 C_{55}^E \end{pmatrix} \begin{pmatrix} \varepsilon_{11} \\ \varepsilon_{22} \\ \gamma_{12} \\ \gamma_{13} \\ \gamma_{23} \end{pmatrix} - \begin{pmatrix} 0 & 0 & \bar{e}_{31} \\ 0 & 0 & \bar{e}_{31} \\ 0 & 0 & 0 \\ e_{15} & 0 & 0 \\ 0 & e_{15} & 0 \end{pmatrix} \begin{pmatrix} E_1 \\ E_2 \\ E_3 \end{pmatrix} \quad (6)$$

in which e represents the permeability constant of piezoelectric material and E_k indicates the components of the electric field. Also C_{ij} is related to the matrix of modulus of elasticity and \bar{C}_{ij}^E are the components of the symmetric piezoelectric stiffness ma-

trix given as following and \bar{e}_{31} is the reduced permeability constant of piezoelectric material given as [18]

$$\begin{aligned} \bar{C}_{11}^E &= C_{11}^E - (C_{13}^E)^2 / C_{33}^E & \bar{C}_{12}^E &= C_{12}^E - (C_{13}^E)^2 / C_{33}^E \\ \bar{e}_{31}^E &= e_{31} - C_{13}^E e_{33} / C_{33}^E \end{aligned}$$

Moreover, the electric displacement-strain relation for the symmetry piezoelectric material is given as [17]

$$\begin{pmatrix} D_1 \\ D_2 \\ D_3 \end{pmatrix} = \begin{pmatrix} 0 & 0 & 0 & e_{15} & 0 \\ 0 & 0 & 0 & 0 & e_{15} \\ \bar{e}_{31} & \bar{e}_{31} & 0 & 0 & 0 \end{pmatrix} \{ \varepsilon_{11} \ \varepsilon_{22} \ \gamma_{12} \ \gamma_{13} \ \gamma_{23} \}^T + \begin{pmatrix} \bar{\Xi}_{11} & 0 & 0 \\ 0 & \bar{\Xi}_{11} & 0 \\ 0 & 0 & \bar{\Xi}_{33} \end{pmatrix} \begin{pmatrix} E_1 \\ E_2 \\ E_3 \end{pmatrix} \quad (7)$$

in which D_i ($i=1\sim3$) represents the components of an electric displacement, $\bar{\Xi}_{11}$, $\bar{\Xi}_{33}$ are the symmetric reduced dielectric constants of piezoelectric layer and

Table 1. Material properties.

Property	FGM	PZT4	
Young's modulus (GPa)	$E_c = 205$	$C_{11}^E = 132$	$C_{12}^E = 71$
	$E_m = 200$	$C_{33}^E = 115$	$C_{13}^E = 73$
		$C_{55}^E = 26$	
Density (kg/m ³)	$\rho_c = 8900$	$\rho_p = 7500$	
	$\rho_m = 7800$		
Poisson ratio	0.3		-
e_{31} (C/m ²)			-4.1
e_{33} (C/m ²)			14.1
e_{15} (C/m ²)			10.5
$\bar{\Xi}_{11}$ (nF/m)			7.124
$\bar{\Xi}_{33}$ (nF/m)			5.841

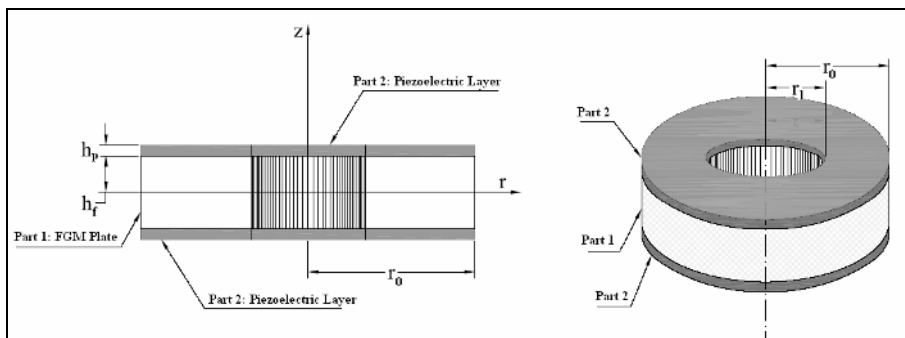


Fig. 1. Schematic representation of the coupled piezo-FGM annular plate.

given as [18]

$$\bar{\Xi}_{33} = \Xi_{33} + (e_{33}^2 / C_{33}^E) \bar{\Xi}_{11} = \Xi_{11}$$

in which Ξ_{33}, Ξ_{11} are the dielectric constants.

3. Constitutive relations

The schematic representation of an annular FG plate with piezoelectric layers mounted on its surfaces is shown in Fig. 1. The cylindrical coordinate system is adopted where the r - θ plane is coincident with the mid-plane of the undeformed plate. Usually, in the analysis of the thick plates, the first order shear deformation plate theory is used in which the effect of the shear deformation and the rotary inertia cannot be omitted. It is assumed that (a) there is no “thickness stretch” of the plate; (b) straight material lines that are perpendicular to the mid-plane in the undeformed state remain straight in the deformed state even though they may not remain perpendicular to the mid-plane. According to this theory, the displacement fields of the plate in the cylindrical coordinate are given as [19]

$$u_z = u_z(r, \theta, t) = w(r, \theta, t) \tag{8}$$

$$u_r = u_r(r, \theta, z, t) = z\psi_r(r, \theta, t) \tag{9}$$

$$u_\theta = u_\theta(r, \theta, z, t) = z\psi_\theta(r, \theta, t) \tag{10}$$

where u_z, u_r and u_θ are the displacements in the transverse z -direction, radial r -direction, and tangential θ -direction of the plate, respectively; w is the transverse displacement of the mid-plane; and ψ_r and ψ_θ are the rotations of vertical lines perpendicular to the mid-plane, measured on the z - r and z - θ planes, respectively.

It is also assumed that the poling direction of the piezoelectric material is in the z -direction. A differential strain can be induced in case of applying external electric potential across the piezoelectric layer, resulting in bending of the plate. The strain of the FG plate and piezoelectric layers in the radial and tangential directions and the shear component are given by Reddy [20] as

$$\epsilon_{rr} = \frac{\partial u_r}{\partial r} = z \frac{\partial \psi_r}{\partial r} \tag{11}$$

$$\epsilon_{\theta\theta} = \frac{\partial u_\theta}{r \partial \theta} + \frac{u_r}{r} = z \left(\frac{\partial \psi_\theta}{r \partial \theta} + \frac{\psi_r}{r} \right) \tag{12}$$

$$\gamma_{r\theta} = \frac{\partial u_r}{r \partial \theta} + \frac{\partial u_\theta}{\partial r} - \frac{u_\theta}{r} = z \left(\frac{\partial \psi_r}{r \partial \theta} - \frac{\psi_\theta}{r} + \frac{\partial \psi_\theta}{\partial r} \right) \tag{13}$$

$$\gamma_{rz} = \frac{\partial u_r}{\partial z} + \frac{\partial u_z}{\partial r} = \psi_r + \frac{\partial w}{\partial r} \tag{14}$$

$$\gamma_{\theta z} = \frac{\partial u_\theta}{\partial z} + \frac{\partial u_z}{r \partial \theta} = \psi_\theta + \frac{\partial w}{r \partial \theta} \tag{15}$$

The stress components in the FG plate in terms of strains or component of displacement field based on the generalized Hooke’s Law are [20]

$$\sigma_{rr}^f = \frac{E(z)}{1-\nu^2} (\epsilon_{rr} + \nu \epsilon_{\theta\theta}) = \frac{zE(z)}{1-\nu^2} \left[\frac{\partial \psi_r}{\partial r} + \nu \left(\frac{\partial \psi_\theta}{r \partial \theta} + \frac{\psi_r}{r} \right) \right] \tag{16a}$$

$$\sigma_{\theta\theta}^f = \frac{E(z)}{1-\nu^2} (\epsilon_{\theta\theta} + \nu \epsilon_{rr}) = \frac{zE(z)}{1-\nu^2} \left[\frac{\psi_r}{r} + \frac{\partial \psi_\theta}{r \partial \theta} + \nu \frac{\partial \psi_r}{\partial r} \right] \tag{16b}$$

$$\tau_{r\theta}^f = \frac{E(z)}{2(1+\nu)} \gamma_{r\theta} = \frac{zE(z)}{2(1+\nu)} \left[\frac{\partial \psi_\theta}{\partial r} - \frac{\psi_\theta}{r} + \frac{\partial \psi_r}{r \partial \theta} \right] \tag{16c}$$

$$\tau_{rz}^f = \kappa^2 \frac{E(z)}{2(1+\nu)} \gamma_{rz} = \kappa^2 \frac{E(z)}{2(1+\nu)} \left[\psi_r + \frac{\partial w}{\partial r} \right] \tag{16d}$$

$$\tau_{\theta z}^f = \kappa^2 \frac{E(z)}{2(1+\nu)} \gamma_{\theta z} = \kappa^2 \frac{E(z)}{2(1+\nu)} \left[\psi_\theta + \frac{\partial w}{r \partial \theta} \right] \tag{16e}$$

where $E(z)$, Young’s modulus, of the FGM material is expressed in Eq. (4) and the shear factor (κ) employed in Mindlin’s plate model [17] to correct for the shear modulus, chosen as $\pi/\sqrt{12}$ here; moreover, the superscript (f) indicates the variable in the FG core plate.

Two piezoelectric layers are attached to the FG plate and intended to be used as an actuator or sensor to determine the natural frequencies of a vibrating coupled plate. There are several different models representing the input electric potential for such a piezoelectric layer. In this paper we decided to adopt the following sinusoidal function for electric potential

proposed by Liu et al. [21], which is appropriate for free vibrations of the proposed system:

$$\phi(r, \theta, z, t) = \varphi(r, \theta, t) \sin(\pi(z - h_f)/h_p) \quad (17)$$

where φ is the electric potential on the mid-surface of the piezoelectric layer; $2h_f$ and h_p are the thickness of the FGM and the piezoelectric layer, respectively; It is noted that the assumed potential function satisfies the boundary conditions that electric potential vanishes at the internal and the external surfaces. Based on the aforementioned assumption of electric potential distribution across the thickness direction shown in Eq. (17), the components of electric field intensity E and electric flux density D can be written in the cylindrical coordinate as [22]

$$E_r = -\frac{\partial \phi}{\partial r} = -\frac{\partial \varphi}{\partial r} \sin \frac{\pi(z - h_f)}{h_p} \quad (18a)$$

$$E_\theta = -\frac{\partial \phi}{r \partial \theta} = -\frac{\partial \varphi}{r \partial \theta} \sin \frac{\pi(z - h_f)}{h_p} \quad (18b)$$

$$E_z = -\frac{\partial \phi}{\partial z} = -\frac{\pi \varphi}{h_p} \cos \frac{\pi(z - h_f)}{h_p} \quad (18c)$$

$$D_r = e_{15} \gamma_{rz} + \bar{\Xi}_{11} E_r = e_{15} \left(\psi_r + \frac{\partial w}{\partial r} \right) - \bar{\Xi}_{11} \frac{\partial \varphi}{\partial r} \sin \frac{\pi(z - h_f)}{h_p} \quad (19a)$$

$$D_\theta = e_{15} \gamma_{\theta z} + \bar{\Xi}_{11} E_\theta = e_{15} \left(\psi_\theta + \frac{\partial w}{r \partial \theta} \right) - \bar{\Xi}_{11} \frac{\partial \varphi}{r \partial \theta} \sin \frac{\pi(z - h_f)}{h_p} \quad (19b)$$

$$D_z = \bar{\Xi}_{33} E_z + \bar{e}_{31} (\epsilon_{rr} + \epsilon_{\theta\theta}) = -\bar{\Xi}_{33} \frac{\pi \varphi}{h_p} \cos \frac{\pi(z - h_f)}{h_p} + z \bar{e}_{31} \left(\frac{\partial \psi_r}{\partial r} + \frac{\psi_r}{r} + \frac{\partial \psi_\theta}{r \partial \theta} \right) \quad (19c)$$

in which E_r, E_θ and E_z are the electric field intensity in the r, θ and z directions, respectively. Also D_r, D_θ and D_z are the corresponding electric displacements in indicated directions; the stress - strain - electric field intensity relations in the piezoelectric layers in the cylindrical coordinate referred to Eq. (6) can be written as:

$$\sigma_{rr}^p = \bar{C}_{11}^E \epsilon_{rr} + \bar{C}_{12}^E \epsilon_{\theta\theta} - \bar{e}_{31} E_z \quad (20a)$$

$$\sigma_{\theta\theta}^p = \bar{C}_{12}^E \epsilon_{rr} + \bar{C}_{11}^E \epsilon_{\theta\theta} - \bar{e}_{31} E_z \quad (20b)$$

$$\tau_{r\theta}^p = \frac{1}{2} (\bar{C}_{11}^E - \bar{C}_{12}^E) \gamma_{r\theta} = z (\bar{C}_{11}^E - \bar{C}_{12}^E) \left(\frac{\partial \psi_r}{r \partial \theta} - \frac{\psi_\theta}{r} + \frac{\partial \psi_\theta}{\partial r} \right) \quad (20c)$$

$$\tau_{rz}^p = \kappa^2 C_{55}^E \gamma_{rz} + e_{15} E_r \quad (20d)$$

$$\tau_{\theta z}^p = \kappa^2 C_{55}^E \gamma_{\theta z} + e_{15} E_\theta \quad (20e)$$

in which the superscript p indicates the parameter under consideration belongs to the piezoelectric layers.

4. Derivation of the governing equations

To obtain the governing differential equation of the coupled piezoelectric annular FGM plate, we begin with resultant moments and resultant shear force components as [23]

$$M_{rr} = \int_{-h_f-h_p}^{h_f+h_p} z \sigma_{rr} dz = \int_{-h_f}^{h_f} z \sigma_{rr}^f dz + 2 \int_{h_f}^{h_f+h_p} z \sigma_{rr}^p dz \quad (21a)$$

$$M_{\theta\theta} = \int_{-h_f-h_p}^{h_f+h_p} z \sigma_{\theta\theta} dz = \int_{-h_f}^{h_f} z \sigma_{\theta\theta}^f dz + 2 \int_{h_f}^{h_f+h_p} z \sigma_{\theta\theta}^p dz \quad (21b)$$

$$M_{r\theta} = \int_{-h_f-h_p}^{h_f+h_p} z \tau_{r\theta} dz = \int_{-h_f}^{h_f} z \tau_{r\theta}^f dz + 2 \int_{h_f}^{h_f+h_p} z \tau_{r\theta}^p dz \quad (21c)$$

$$Q_r = \int_{-h_f-h_p}^{h_f+h_p} \tau_{rz} dz = \int_{-h_f}^{h_f} \tau_{rz}^f dz + 2 \int_{h_f}^{h_f+h_p} \tau_{rz}^p dz \quad (22a)$$

$$Q_\theta = \int_{-h_f-h_p}^{h_f+h_p} \tau_{\theta z} dz = \int_{-h_f}^{h_f} \tau_{\theta z}^f dz + 2 \int_{h_f}^{h_f+h_p} \tau_{\theta z}^p dz \quad (22b)$$

Now by substituting the stress components in terms of displacement components Eqs. (14)-(16) and Eqs. (20) in Eqs. (21), (22) and carry out the integrations, one would get the resultant moments and shear force components caused by the stresses as:

$$M_{rr} = \left[(d_1 + d_2) \frac{\partial \psi_r}{\partial r} + (d_1 + d_2 - 2A_1) \left(\frac{\partial \psi_\theta}{r \partial \theta} + \frac{\psi_r}{r} \right) - \frac{4}{\pi} h_p \bar{e}_{31} \varphi \right] \quad (23a)$$

$$M_{\theta\theta} = \left[(d_1 + d_2 - 2A_1) \frac{\partial \psi_r}{\partial r} + (d_1 + d_2) \left(\frac{\partial \psi_\theta}{r \partial \theta} + \frac{\psi_r}{r} \right) - \frac{4}{\pi} h_p \bar{e}_{31} \varphi \right] \quad (23b)$$

$$M_{r\theta} = A_1 \left(\frac{\partial \psi_r}{r \partial \theta} + \frac{\partial \psi_\theta}{\partial r} - \frac{\psi_\theta}{r} \right) \quad (23c)$$

$$Q_r = A_3 \left(\frac{\partial w}{\partial r} + \psi_r \right) - \frac{4}{\pi} h_p e_{15} \frac{\partial \varphi}{\partial r} \quad (24a)$$

$$Q_\theta = A_3 \left(\frac{\partial w}{r \partial \theta} + \psi_\theta \right) - \frac{4}{\pi} h_p e_{15} \frac{\partial \varphi}{r \partial \theta} \quad (24b)$$

where the coefficients of d_1 , d_2 , A_1 and A_3 in the above equations are related to plate stiffness and are given by

$$d_1 = \int_{-h_f}^{h_f} \frac{z^2 E_f(z)}{1 - \nu_f^2} dz \quad (25a)$$

$$d_2 = 2 \int_{h_f}^{h_f+h_p} \bar{C}_{11}^E z^2 dz \quad (25b)$$

$$A_1 = \frac{1}{2} \left[\left((1 - \nu) d_1 + \left(1 - \frac{\bar{C}_{12}^E}{\bar{C}_{11}^E} \right) d_2 \right) \right] \quad (26a)$$

$$A_3 = \frac{1}{2} \int_{-h_f}^{h_f} \frac{\kappa^2 E(z)}{(1 + \nu)} dz + 2 \kappa^2 C_{55}^E h_p \quad (26b)$$

M_{rr} , $M_{r\theta}$, $M_{\theta\theta}$, Q_r and Q_θ must satisfy the following dynamic equilibrium equations [21]:

$$\frac{\partial Q_r}{\partial r} + \frac{\partial Q_\theta}{r \partial \theta} + \frac{Q_r}{r} - \quad (27a)$$

$$\left(\int_{-h_f}^{h_f} \rho_f(z) \frac{\partial^2 u_z}{\partial t^2} dz + 2 \int_{h_f}^{h_f+h_p} \rho_p \frac{\partial^2 u_z}{\partial t^2} dz \right) = 0$$

$$\frac{\partial M_{rr}}{\partial r} + \frac{\partial M_{r\theta}}{r \partial \theta} + \frac{M_{rr} - M_{\theta\theta}}{r} - Q_r - \quad (27b)$$

$$\left(\int_{-h_f}^{h_f} z \rho_f(z) \frac{\partial^2 u_r}{\partial t^2} dz + 2 \int_{h_f}^{h_f+h_p} z \rho_p \frac{\partial^2 u_r}{\partial t^2} dz \right) = 0$$

$$\frac{\partial M_{r\theta}}{\partial r} + \frac{\partial M_{\theta\theta}}{r \partial \theta} + \frac{2M_{r\theta}}{r} - Q_\theta - \quad (27c)$$

$$\left(\int_{-h_f}^{h_f} z \rho_f(z) \frac{\partial^2 u_\theta}{\partial t^2} dz + 2 \int_{h_f}^{h_f+h_p} z \rho_p \frac{\partial^2 u_\theta}{\partial t^2} dz \right) = 0$$

where ρ_f and ρ_p are material densities of the FG plate and piezoelectric layer, respectively.

Note that all of the electrical variables primarily must satisfy Maxwell's equation which requires that the divergence of the electric flux density vanishes at any point within the media. This condition can be satisfied by enforcing the integration of the electric flux divergence across the thickness of the piezoelectric layers to be zero for any r and θ as [22]

$$\int_{h_f}^{h_f+h_p} \bar{\nabla} \cdot \bar{D} dz = \int_{h_f}^{h_f+h_p} \left(\frac{\partial(rD_r)}{r \partial r} + \frac{\partial D_\theta}{r \partial \theta} + \frac{\partial D_z}{\partial z} \right) dz = 0 \quad (28)$$

The operator $\bar{\nabla}$ in the above equation is the gradient operator in the polar coordinate.

Now we assume that the rotations ψ_r and ψ_θ are expressed in terms of the potential functions $H(r, \theta, t)$ and $R(r, \theta, t)$ as through the following transformation [19]:

$$\psi_r = \frac{\partial R}{\partial r} + \frac{\partial H}{r \partial \theta} \quad \psi_\theta = \frac{\partial R}{r \partial \theta} - \frac{\partial H}{\partial r} \quad (29a,b)$$

It is assumed that solutions of w , R , H , and φ for wave propagation in the θ direction take the form:

$$\begin{aligned} w(r, \theta, t) &= w_1(r) \cos(m\theta) e^{i\omega t} \\ R(r, \theta, t) &= R_1(r) \cos(m\theta) e^{i\omega t} \\ H(r, \theta, t) &= H_1(r) \sin(m\theta) e^{i\omega t} \\ \varphi(r, \theta, t) &= \varphi_1(r) \cos(m\theta) e^{i\omega t} \end{aligned} \quad (30a-d)$$

where m is the number of nodal diameters and $w_1(r)$, $R_1(r)$, $H_1(r)$ and $\varphi_1(r)$ are amplitudes of $w(r, \theta, t)$, $R(r, \theta, t)$, $H(r, \theta, t)$ and $\varphi(r, \theta, t)$ respectively.

Eqs. (30a-d) are adopted as they represent harmonic oscillation and are consistent with the assumption that the plate undergoes small synchronous free vibratory motions. To satisfy Eqs. (27a-c), the sine instead of cosine function is employed for $H(r, \theta, t)$. Substituting Eqs. (29a, b) and (30a-d) into Eqs. (27a-c) and (28) reduces to

$$A_3 \bar{\Delta} R_1 + A_3 \bar{\Delta} w_1 + A_2 \omega^2 w_1 - A_6 \bar{\Delta} \varphi_1 = 0 \quad (31a)$$

$$\begin{aligned} \frac{\partial}{\partial r} \left[(d_1 + d_2) \bar{\Delta} R_1 - (A_3 - A_4 \omega^2) R_1 - A_3 w_1 + A_5 \varphi_1 \right] \\ + \frac{m}{r} \left[A_4 \bar{\Delta} H_1 - (A_3 - A_4 \omega^2) H_1 \right] = 0 \end{aligned} \quad (31b)$$

$$\begin{aligned} \frac{m}{r} \left[(d_1 + d_2) \bar{\Delta} R_1 - (A_3 - A_4 \omega^2) R_1 - A_3 w_1 + A_5 \varphi_1 \right] \\ + \frac{\partial}{\partial r} \left[A_4 \bar{\Delta} H_1 - (A_3 - A_4 \omega^2) H_1 \right] = 0 \end{aligned} \quad (31c)$$

$$\bar{\Delta} R_1 + A_7 \bar{\Delta} w_1 - A_8 \bar{\Delta} \varphi_1 + A_5 \varphi_1 = 0 \quad (31d)$$

where

$$\bar{\Delta} = \frac{\partial^2}{\partial r^2} + \frac{\partial}{r \partial r} - \frac{m^2}{r^2}, \quad A_2 = 2 \rho_p h_p + \int_{-h_f}^{h_f} \rho_f(z) dz$$

$$A_4 = \int_{-h_f}^{h_f} z^2 \rho_f(z) dz + 2/3 \rho_p [(h_f + h_p)^3 - h_f^3], \quad \frac{A_6 y}{A_8 y - x - A_7} = \lambda \tag{35a,b}$$

$$A_5 = \frac{4h_p(e_{15} - \bar{e}_{31})}{\pi}, \quad A_6 = \frac{4h_p e_{15}}{\pi}, \quad A_7 = \frac{e_{15}}{e_{15} + \bar{e}_{31}},$$

$$A_8 = \frac{2\bar{\bar{e}}_{11}}{\pi(e_{15} + \bar{e}_{31})}, \quad A_9 = \frac{2\pi \bar{\bar{e}}_{11}}{h_p^2(e_{15} + \bar{e}_{31})}$$

where λ is a constant. Under the above condition, Eq. (34) can be thus reduced to

$$\Delta w_1 - \lambda w_1 = 0 \tag{36}$$

5. Solution method

In the four differential equations of motion, Eqs. (31a-d), there are four independent variables w , R , H and φ that need to be defined. The solution procedure is described hereafter. H_1 can be separated from R_1 and w_1 by differentiation, addition, and subtraction of Eqs. (31b,c). These two equations become

$$\bar{\Delta} [A_4 \bar{\Delta} H_1 - (A_3 - A_4 \omega^2) H_1] = 0 \tag{32a}$$

$$\bar{\Delta} [(d_1 + d_2) \bar{\Delta} R_1 - (A_3 - A_4 \omega^2) R_1 - A_3 w_1 + A_5 \varphi_1] = 0 \tag{32b}$$

We first adopt the following transformation of variable, similar to that in references [19,24] to uncouple R_1 , w_1 and φ_1 in Eqs. (31a,d) and (32b):

$$R_1 = x w_1$$

$$\varphi_1 = y w_1 \tag{33a,b}$$

where x, y are constants. Substituting Eqs. (33) into (31a,d) and (32b), these equations can be simplified as follows:

$$\bar{\Delta} \left[\bar{\Delta} w_1 - \frac{A_3 - A_5 y + (A_3 - A_4 \omega^2) x}{(d_1 + d_2) x} w_1 \right] = 0, \tag{34a}$$

$$\bar{\Delta} w_1 - \frac{A_2 \omega^2}{A_6 y - A_3(x+1)} w_1 = 0, \tag{34b}$$

$$\bar{\Delta} w_1 - \frac{A_6 y}{A_8 y - x - A_7} w_1 = 0, \tag{34c}$$

It can be observed that the terms within the brackets in Eqs. (34a,b) and (34c) are of identical form. Hence, for the solution of w_1 to be unique, we have

$$\frac{A_3 - A_5 y + (A_3 - A_4 \omega^2) x}{(d_1 + d_2) x} = \frac{A_2 \omega^2}{A_6 y - A_3(x+1)} = \frac{A_6 y}{A_8 y - x - A_7}$$

Eq. (35a) is cubic in x and y , which gives three roots, x_i, y_i ($i=1\sim 3$) from which λ_i ($i=1\sim 3$) can be calculated correspondingly from Eq. (35b). Three sets of Bessel functions $c_i Z_{i1}(m, \alpha_i r) + c_{i+3} Z_{i2}(m, \alpha_i r)$, ($i=1\sim 3$) where $\alpha_i = \sqrt{|\lambda_i|}$ can be obtained by substituting λ_i into Eq. (36). The final solutions are given as

$$w = \sum_{i=1}^3 [c_i Z_{i1}(m, \alpha_i r) + c_{i+3} Z_{i2}(m, \alpha_i r)] \cos(m\theta) e^{i\omega t} \tag{37a}$$

$$R = \sum_{i=1}^3 x_i [c_i Z_{i1}(m, \alpha_i r) + c_{i+3} Z_{i2}(m, \alpha_i r)] \cos(m\theta) e^{i\omega t} \tag{37b}$$

$$\varphi = \sum_{i=1}^3 y_i [c_i Z_{i1}(m, \alpha_i r) + c_{i+3} Z_{i2}(m, \alpha_i r)] \cos(m\theta) e^{i\omega t} \tag{37c}$$

where

$$Z_{i1}(m, \alpha_i r) = \begin{cases} J_m(\alpha_i r) & , \lambda_i < 0 \\ I_m(\alpha_i r) & , \lambda_i > 0 \end{cases} \quad (i = 1, 2, 3) \tag{38}$$

$$Z_{i2}(m, \alpha_i r) = \begin{cases} Y_m(\alpha_i r) & , \lambda_i < 0 \\ K_m(\alpha_i r) & , \lambda_i > 0 \end{cases} \quad (i = 1, 2, 3)$$

where J and Y are Bessel functions of the first and second kind, respectively; I and K are modified Bessel functions of the first and second kind, respectively, and c_i ($i=1-6$) are six constants of integration.

Substituting Eq. (34a) into Eqs. (31b,c), gives the following Bessel equation:

$$\Delta H_1 - \lambda_4 H_1 = 0 \tag{39}$$

where

$$\lambda_4 = \frac{A_3 - A_4 \omega^2}{A_1}$$

Finally, H can be expressed as

$$H = [c_7 Z_{41}(m, \alpha_4 r) + c_8 Z_{42}(m, \alpha_4 r)] \sin(m\theta) e^{i\omega t} \tag{40}$$

where $\alpha_4 = \sqrt{|\lambda_4|}$ and the definition of $Z_{41}(m, \alpha_4 r)$ and $Z_{42}(m, \alpha_4 r)$ is the same as Eq. (43); and c_i ($i=7,8$) are integration constants. Substituting Eqs. (37a-c) and (40) into Eqs. (29) gives

$$\psi_r = \left[\sum_{i=1}^3 x_i \left(c_i \frac{\partial Z_{i1}}{\partial r} + c_{i+3} \frac{\partial Z_{i2}}{\partial r} \right) + \frac{m}{r} (c_7 Z_{41} + c_8 Z_{42}) \right] \cos(m\theta) e^{i\omega t} \tag{41a}$$

$$\psi_\theta = - \left[\frac{m}{r} \sum_{i=1}^3 x_i (c_i Z_{i1} + c_{i+3} Z_{i2}) + \left(c_7 \frac{\partial Z_{41}}{\partial r} + c_8 \frac{\partial Z_{42}}{\partial r} \right) \right] \sin(m\theta) e^{i\omega t} \tag{41b}$$

As usual, the determinant of the matrix containing the system frequencies is generated after the electric and displacement boundary conditions are imposed. If the plate is insulated at the edge, the electrical flux conservation equation is given by

$$\int_{h_f}^{h_b} D_r(r, \theta, t) dz = 0 \tag{42}$$

The electric boundary condition can be obtained by substituting Eq. (19a) into Eq. (42) giving

$$\psi_r + \frac{\partial w}{\partial r} - \frac{2\Xi_{11}}{\pi e_{15}} \frac{\partial \varphi}{\partial r} = 0 \tag{43}$$

The standard boundary conditions for the clamped, simply supported (soft type) and free edges are given respectively as follows:

(i) Clamped:

$$\begin{pmatrix} Z_{11}(\alpha_1 r_1) & Z_{12}(\alpha_1 r_1) & Z_{21}(\alpha_2 r_1) & Z_{22}(\alpha_2 r_1) & Z_{31}(\alpha_3 r_1) & Z_{32}(\alpha_3 r_1) & 0 & 0 \\ x_1 Z'_{11}(\alpha_1 r_1) & x_1 Z'_{12}(\alpha_1 r_1) & x_2 Z'_{21}(\alpha_2 r_1) & x_2 Z'_{22}(\alpha_2 r_1) & x_3 Z'_{31}(\alpha_3 r_1) & x_3 Z'_{32}(\alpha_3 r_1) & \frac{m}{r_1} Z_{41}(\alpha_4 r_1) & \frac{m}{r_1} Z_{42}(\alpha_4 r_1) \\ \frac{mx_1}{r_1} Z_{11}(\alpha_1 r_1) & \frac{mx_1}{r_1} Z_{12}(\alpha_1 r_1) & \frac{mx_2}{r_1} Z_{21}(\alpha_2 r_1) & \frac{mx_2}{r_1} Z_{22}(\alpha_2 r_1) & \frac{mx_3}{r_1} Z_{31}(\alpha_3 r_1) & \frac{mx_3}{r_1} Z_{32}(\alpha_3 r_1) & r_1 Z'_{41}(\alpha_4 r_1) & r_1 Z'_{42}(\alpha_4 r_1) \\ \varphi_{11}(r_1) & \varphi_{12}(r_1) & \varphi_{21}(r_1) & \varphi_{22}(r_1) & \varphi_{31}(r_1) & \varphi_{32}(r_1) & 0 & 0 \\ Z_{11}(\alpha_1 r_0) & Z_{12}(\alpha_1 r_0) & Z_{21}(\alpha_2 r_0) & Z_{22}(\alpha_2 r_0) & Z_{31}(\alpha_3 r_0) & Z_{32}(\alpha_3 r_0) & 0 & 0 \\ x_1 Z'_{11}(\alpha_1 r_0) & x_1 Z'_{12}(\alpha_1 r_0) & x_2 Z'_{21}(\alpha_2 r_0) & x_2 Z'_{22}(\alpha_2 r_0) & x_3 Z'_{31}(\alpha_3 r_0) & x_3 Z'_{32}(\alpha_3 r_0) & \frac{m}{r_0} Z_{41}(\alpha_4 r_0) & \frac{m}{r_0} Z_{42}(\alpha_4 r_0) \\ \frac{mx_1}{r_0} Z_{11}(\alpha_1 r_0) & \frac{mx_1}{r_0} Z_{12}(\alpha_1 r_0) & \frac{mx_2}{r_0} Z_{21}(\alpha_2 r_0) & \frac{mx_2}{r_0} Z_{22}(\alpha_2 r_0) & \frac{mx_3}{r_0} Z_{31}(\alpha_3 r_0) & \frac{mx_3}{r_0} Z_{32}(\alpha_3 r_0) & r_0 Z'_{41}(\alpha_4 r_0) & r_0 Z'_{42}(\alpha_4 r_0) \\ \varphi_{11}(r_0) & \varphi_{12}(r_0) & \varphi_{21}(r_0) & \varphi_{22}(r_0) & \varphi_{31}(r_0) & \varphi_{32}(r_0) & 0 & 0 \end{pmatrix} \tag{47}$$

$$\begin{aligned} w(r_1, \theta, t) &= \psi_r(r_1, \theta, t) = \psi_\theta(r_1, \theta, t) \\ &= \left[\pi e_{15} \left(\psi_r + \frac{\partial w}{\partial r} \right) - 2\Xi_{11} \frac{\partial \varphi}{\partial r} \right]_{r=r_1} = 0, \\ w(r_0, \theta, t) &= \psi_r(r_0, \theta, t) = \psi_\theta(r_0, \theta, t) \\ &= \left[\pi e_{15} \left(\psi_r + \frac{\partial w}{\partial r} \right) - 2\Xi_{11} \frac{\partial \varphi}{\partial r} \right]_{r=r_0} = 0 \end{aligned} \tag{44a,b}$$

(ii) Simply supported (soft type):

$$\begin{aligned} w(r_1, \theta, t) &= M_{rr}(r_1, \theta, t) = M_{r\theta}(r_1, \theta, t) \\ &= \left[\pi e_{15} \left(\psi_r + \frac{\partial w}{\partial r} \right) - 2\Xi_{11} \frac{\partial \varphi}{\partial r} \right]_{r=r_1} = 0 \\ w(r_0, \theta, t) &= M_{rr}(r_0, \theta, t) = M_{r\theta}(r_0, \theta, t) \\ &= \left[\pi e_{15} \left(\psi_r + \frac{\partial w}{\partial r} \right) - 2\Xi_{11} \frac{\partial \varphi}{\partial r} \right]_{r=r_0} = 0 \end{aligned} \tag{45a,b}$$

(iii) Free:

$$\begin{aligned} M_{rr}(r_1, \theta, t) &= M_{r\theta}(r_1, \theta, t) = Q_r(r_1, \theta, t) \\ &= \left[\pi e_{15} \left(\psi_r + \frac{\partial w}{\partial r} \right) - 2\Xi_{11} \frac{\partial \varphi}{\partial r} \right]_{r=r_1} = 0 \\ M_{rr}(r_0, \theta, t) &= M_{r\theta}(r_0, \theta, t) = Q_r(r_0, \theta, t) \\ &= \left[\pi e_{15} \left(\psi_r + \frac{\partial w}{\partial r} \right) - 2\Xi_{11} \frac{\partial \varphi}{\partial r} \right]_{r=r_0} = 0 \end{aligned} \tag{46a,b}$$

For all possible combinations of clamped, simply supported and free edge conditions at the inner ($r=r_1$) and outer ($r=r_0$) circular boundaries of the annular plate (Fig. 1), a matrix involving the system frequencies can always be formulated. For example, the determinant of frequencies under clamped-clamped (C-C) boundary condition is given by substituting Eqs. (37a,c) and (41) into Eq. (44), resulting in where $Z_{ij}(m, \alpha_i r_i)$ is expressed as $Z_{ij}(\alpha_i r_i)$ for concise notation, the factors $\cos(m\theta)e^{i\omega t}$ and $\sin(m\theta)e^{i\omega t}$ have been omitted; prime ' denotes $\partial/\partial r$, and

Table 2. Frequencies (Hz) of piezo coupled FG annular plate under C-C and S-S boundary conditions for $r_0/h_f=20$.

Power Index	Mode no.	C*-C boundary conditions				S-S boundary conditions			
		Present FEM	Present Analytical FSDT	Difference (%)	[25]	Present FEM	Present Analytical FSDT	Difference (%)	[25]
0	0	447.54	440.20	-1.64	440.70	222.02	220.60	-0.64	220.91
	1	1218.97	1195.56	-1.92	1196.37	823.31	814.42	-1.08	814.08
	2	2348.01	2298.24	-2.12	2296.29	1795.75	1769.17	-1.48	1768.85
1	0	435.35	428.60	-1.55	-	216.34	215.13	-0.56	-
	1	1185.76	1163.35	-1.89	-	803.66	793.69	-1.24	-
	2	2284.05	2232.89	-2.24	-	1753.12	1726.12	-1.54	-
3	0	429.11	422.63	-1.51	-	214.28	212.84	-0.67	-
	1	1168.76	1147.84	-1.79	-	794.09	783.53	-1.33	-
	2	2251.31	2201.11	-2.23	-	1732.33	1706.00	-1.52	-
5	0	427.24	420.36	-1.61	-	213.29	211.29	-0.94	-
	1	1163.66	1141.32	-1.92	-	791.18	782.56	-1.09	-
	2	2241.47	2189.24	-2.33	-	1725.61	1697.83	-1.61	-
7	0	426.36	420.22	-1.44	-	213.05	211.09	-0.92	-
	1	1161.28	1141.65	-1.69	-	790.06	779.32	-1.36	-
	2	2236.89	2189.02	-2.14	-	1723.22	1695.99	-1.58	-
9	0	425.85	419.25	-1.55	-	212.73	210.96	-0.83	-
	1	1159.87	1137.72	-1.91	-	788.91	778.97	-1.26	-
	2	2234.17	2184.35	-2.23	-	1720.63	1690.86	-1.73	-
10	0	425.68	418.61	-1.66	-	212.64	210.53	-0.99	-
	1	1159.43	1136.47	-1.98	-	788.55	779.01	-1.21	-
	2	2233.33	2180.18	-2.38	-	1719.83	1691.28	-1.66	-

* First letter denotes edge condition at inner edge, C=clamped, S= simply supported

$$\varphi_{ij}(r_0) = \pi e_{15} x_i Z_{ij}(m, \alpha, r_0) + (\pi e_{15} - 2\Xi_{11} y_i) Z'_{ij}(m, \alpha, r_0)'$$

$$\varphi_{ij}(r_1) = \pi e_{15} x_i Z_{ij}(m, \alpha, r_1) + (\pi e_{15} - 2\Xi_{11} y_i) Z'_{ij}(m, \alpha, r_1)'$$

$i = 1, 2, 3, j = 1, 2$

Setting Eq. (47) to zero yields the resonant frequencies and their corresponding mode shapes.

Before going further into the results and discussions, primarily we have to make sure that the obtained results are valid. To do this, initially for some special cases, results are compared with those given in the literature [25].

In the next step, since there were no published results for the hybrid piezoelectric FGM plate we decided to verify the validity of obtained results with those of FEM results. Our FEM model for the piezo-

FG plate comprises a 3D 8-noded solid element with 3 DOF per node (translation) in the core FG plate element and 6 DOF per node (3 translation, temperature, voltage and magnetic properties) in the piezoelectric element.

6. Case studies, results and discussions

To solve the above relations, in this section, a piezoelectric bonded annular FG plate (as shown in Fig.1) is considered under four types of boundary conditions: C-C, S-S, C-S and S-C, where the first and second letter denotes the edge condition at the inner and outer edge, respectively; C denotes clamped and S denotes simply supported boundary conditions. The material parameters of the FGM plate and piezoelectric layers used in the numerical example are listed in Table. 1. The inner radius (r_i) and outer radius (r_o) of the annular plate are 0.1 m and 0.6 m,

Table 3. Frequencies (Hz) of piezo coupled FG annular plate under C-S and S-C boundary conditions for $r_0/h_f=20$.

Power Index	Mode no.	C*-S boundary conditions				S-C boundary conditions			
		Present FEM	Present Analytical FSDT	Diff. (%)	[25]	Present FEM	Present Analytical FSDT	Diff. (%)	[25]
0	0	294.12	291.68	-0.83	290.14	352.21	349.25	-0.84	349.19
	1	981.03	968.87	-1.24	965.43	1041.51	1028.28	-1.27	1027.35
	2	2032.41	1996.44	-1.77	1993.10	2095.91	2060.49	-1.69	2058.51
1	0	287.16	284.83	-0.81	-	343.88	341.06	-0.82	-
	1	957.82	945.27	-1.31	-	1016.87	1004.26	-1.24	-
	2	1984.33	1949.80	-1.74	-	2046.33	2012.16	-1.67	-
3	0	283.72	281.48	-0.79	-	339.76	336.77	-0.88	-
	1	946.36	934.15	-1.29	-	1004.70	991.24	-1.34	-
	2	1960.59	1926.67	-1.73	-	2021.85	1987.07	-1.72	-
5	0	282.62	280.30	-0.82	-	338.44	335.26	-0.94	-
	1	942.68	930.80	-1.26	-	1000.80	986.89	-1.39	-
	2	1952.96	1918.00	-1.79	-	2013.99	1977.94	-1.79	-
7	0	282.24	279.84	-0.85	-	337.99	334.88	-0.92	-
	1	941.41	929.08	-1.31	-	999.45	985.86	-1.36	-
	2	1950.33	1915.03	-1.81	-	2011.26	1975.66	-1.77	-
9	0	281.82	279.48	-0.83	-	337.48	334.68	-0.83	-
	1	940.02	928.27	-1.25	-	997.94	985.47	-1.25	-
	2	1947.40	1912.15	-1.81	-	2008.24	1973.70	-1.72	-
10	0	281.69	279.46	-0.79	-	337.32	333.98	-0.99	-
	1	939.57	926.98	-1.34	-	997.49	983.92	-1.36	-
	2	1946.52	1910.90	-1.83	-	2007.33	1971.00	-1.81	-

* First letter denotes edge condition at inner edge, C=clamped, S=simply supported.

respectively and the thickness ratio of the piezoelectric layer to the FG core plate is 1/10. The thickness of FG core plate is chosen to be 0.03m. The piezoelectric layers are poled in the thickness direction and both surfaces of each layer are short-circuited. Table 2 and Table 3 list the first three frequencies calculated for piezoelectric bounded FG plate achieved by proposed analytical method and by 3D FEA for C-C and S-S as well as C-S and S-C edge boundary conditions.

As one can see from Tables 2 and 3, the obtained results from the proposed analytical method when $g=0$ (isotropic steel plate) corresponds closely with the results of reference [25] and FEM solution. As it is seen in Table 2 the maximum estimated difference between our solution and FEM is about -2.38% for the case where $m=2$, $g=10$ under C-C boundary condition and -1.73% for the case where $m=2$, $g=9$ under S-S boundary condition case. Also, according to the results presented in Table 3, under the C-S boundary

condition the maximum estimated error of our solution with FEM is about -1.83% for the case where $m=2$, $g=10$ and it is -1.81% for the case where $m=2$, $g=10$ under the S-C boundary condition. After verification of the results, we start discussing the obtained results from the closed form solution and the FEM results. The analytical results of the proposed method are closer to the FE analysis results at lower frequencies than they are at higher frequencies as shown in Table 2 and Table 3. For example, the proposed analytical method gives a frequency 1.64% lesser than that of the FE analysis for $g=0$ and $m=0$, while it gives a value of only 2.12% lesser than that of the FE analysis for $g=0$ and $m=2$ under the C-C boundary condition. Also, for the case of the C-S boundary condition according to Table 3, the proposed method gives a frequency 0.83% lesser than that of the FE analysis for $g=0$ and $m=0$, while it gives a value of only 1.77% lesser than that of the FE analysis for $g=0$

and $m=2$ under C–S boundary condition. Moreover, S–S boundary conditions yield smaller frequencies than those under the C–C, C–S and S–C boundary conditions.

In the next step we try to investigate the effect of FGM power index (g) on the natural frequencies of the hybrid plate. The obtained results in Table 2 and Table 3 indicate that by increasing the value of g , the frequency of the system decreases for all types of boundary conditions in all different vibrational modes. Moreover, this decreasing trend of frequency for smaller values of g is more pronounced; for example, in the case of the C–C plate by increasing value of g from 1 to 3 (about 200%) the frequency of the first mode for the hybrid plate decreases by 1.36%, but by increasing g from 3 to 9 (about 200%) of the same plate and for the same mode, the frequency decreases by 0.80%. It is also observed that for the FG plate under the S–S boundary condition by increasing g from 0 to 3 the frequency decreases in the third mode of vibration about 3.57%, but by increasing g from 5 to 10, the frequency decreases for the same plate and the same mode about 0.39%. In the case of the C–S plate by increasing value of g from 1 to 3 (about 200%) the frequency of the first mode for the hybrid plate decreases by 1.18%, but by increasing g from 3 to 9 (about 200%) of the same plate and for the same mode, the frequency decreases by 0.71%. Whereas, it is also observed that for the FG plate in the case of the S–C boundary condition by increasing g from 0 to 3 the frequency decreases in the third mode of vibration about 3.56%, but by increasing g from 5 to 10, the frequency decreases for the same plate and the same mode about 0.35%. To see better the effect of g variations on the natural frequencies of the different plates, Figs. 2 to 5 also illustrate these variations for the first and second mode shapes. As it is seen from Figs. 2 to 5, the behavior of the system follows the same trend in all different cases, i.e., the natural frequencies of the system decrease by increasing of g and stabilizes for g values greater than 7. In fact, for $g \gg 1$ the FGM plate becomes a metal plate and the hybrid plate transforms to a laminated plate with metal core as a host plate.

7. Concluding remarks

An analytical solution for free flexural vibration of a three-layered piezoelectric laminated annular FGM plate is proposed based on FSDPT. Results indicate

that the analytical results of the proposed method are closer to the FE analysis results at lower frequencies than at higher frequencies. Moreover, the S–S boundary conditions yield smaller frequencies than those under C–C, C–S and S–C boundary conditions. It is also observed from the obtained results that by increasing the value of FGM power index (g), the frequency of system decreases for all types of boundary conditions in all different vibrational modes. The analytical solutions and findings contribute towards a simplified model for the parametric study and understanding of vibration of piezoelectric-coupled FG annular plate. It is further shown that for vibrating annular hybrid plates with specified dimensions, one can select a specific piezo-FG plate which can fulfill the designated natural frequency. The analytical solutions provided and the findings will be used in the design of piezoelectric materials in mechanical systems for practical applications, such as the ultrasonic motors.

References

- [1] L. Wang and N. Noda, Design of smart functionally graded thermo-piezoelectric composite structure, *Smart Mater. Struct.*, 10 (2001) 189-193.
- [2] X. Q. He, T. Y. Ng, S. Sivashanker and K. M. Liew, Active control of FGM plates with integrated piezoelectric sensors and actuators, *Int. J. Solids Struct.*, 38 (2001) 1641-1655.
- [3] K. M. Liew, J. Yang and S. Kitipornchai, Post buckling of piezoelectric FGM plates subject to thermo-electro-mechanical loading, *Int. J. Solids Struct.* 40 (2003) 3869-3892.
- [4] H. S. Shen, Post buckling of FGM plates with piezoelectric actuators under thermo-electro-mechanical loadings, *Int. J. Solids Struct.* 42 (2005) 6101-6121.
- [5] J. Yang, S. Kitipornchai and K. M. Liew, Nonlinear analysis of thermo-electro-mechanical behavior of shear deformable FGM plates with piezoelectric actuators, *Int. J. Numer. Methods Eng.*, 59 (2004) 1605-1632.
- [6] J. Yang, S. Kitipornchai and K. M. Liew, Large amplitude vibration of thermo-electric-mechanically stressed FGM laminated plates, *Computer Methods in Applied Mechanics and Engineering*, 192 (2003) 3861-3885.
- [7] X. L. Huang and H. S. Shen, Vibration and dynamic response of functionally graded plates with

- piezoelectric actuators in thermal environments, *J. Sound Vib.*, 289 (2006) 25-53.
- [8] F. Ebrahimi and A. Rastgoo, Free vibration analysis of smart annular FGM plates integrated with piezoelectric layers, *Smart Mater. Struct.*, 17 (2008) no. 015044.
- [9] F. Ebrahimi and A. Rastgoo, An analytical study on the free vibration of smart circular thin FGM plate based on classical plate theory, *Thin-Walled Structures*, 46 (2008) 1402–1408.
- [10] F. Ebrahimi, A. Rastgoo and M. H. Kargarnovin, Analytical investigation on axisymmetric free vibrations of moderately thick circular functionally graded plate integrated with piezoelectric layers, *Journal of mechanical science and technology*, 22 (2008) 1058-1072.
- [11] F. Ebrahimi and A. Rastgoo, Free Vibration Analysis of Smart FGM Plates, *International Journal of Mechanical Systems Science and Engineering*, 2 (2) (2008) 94-99.
- [12] F. Ebrahimi and A. Rastgoo, Nonlinear vibration of smart circular functionally graded plates coupled with piezoelectric layers, *International Journal of Mechanics and Materials in Design*, published online: 11 Jan. 2009.
- [13] J. Markworth, K. S. Ramesh and Jr. Parks, Modeling studies applied to functionally graded materials, *J. Mater. Sci.*, 30 (1995) 2183-2193.
- [14] J. N. Reddy and G. N. Praveen, Nonlinear transient thermoelastic analysis of functionally graded ceramic-metal plate, *Int. J. Solids Struct.*, 35 (1998) 4457-4476.
- [15] R. C. Wetherhold and S. Wang, The use of functionally graded materials to eliminate or thermal deformation, *Composite Sci. Tech.*, 56 (1996) 1099-1104.
- [16] Y. Tanigawa, H. Morishita and S. Ogaki, Derivation of system of fundamental equations for a three dimensional thermoelastic field with nonhomogeneous material properties and its application to a semi infinite body, *J. Thermal Stress*, 22 (1999) 689-711.
- [17] H. F. Tiersten, *Linear piezoelectric plate vibrations*, plenum press, New York, USA, (1969).
- [18] Q. Wang, S. T. Quek and X. Liu, Analysis of piezoelectric coupled circular plate, *Smart Mater Struct.*, 10 (2001) 229-239.
- [19] R. D. Mindlin, Influence of rotary inertia and shear on flexural motions of isotropic elastic plates, *J. Appl Mech.*, 18 (1951) 31-38.
- [20] J. N. Reddy, *Theory and analysis of elastic plates*, Taylor and Francis, Philadelphia, USA, (1999).
- [21] X. Liu, Q. Wang and S. T. Quek, Analytical solution for free vibration of piezoelectric coupled moderately thick circular plates, *Int. J. Solids Struct.*, 39 (2002) 2129-2151.
- [22] D. Halliday and R. Resnick, *Physics*, John Wiley and Sons, New York, USA, (1978).
- [23] D. O. Brush and B. O. Almroth, *Buckling of bars plates and shells*, McGraw-Hill, New York, USA, (1975).
- [24] H. J. Ding, B. J. Chen and J. Liang, General solutions for coupled equations for piezoelectric media, *Int. J. Solids Struct.*, 33 (1996) 2283–98.
- [25] W. H. Duan, S. T. Quek and Q. Wang, Free vibration analysis of piezoelectric coupled thin and thick annular plate, *J. Sound Vib.*, 281 (2005) 119–39.



Farzad Ebrahimi received his B.S. and M.S. degree in Mechanical Engineering from University of Tehran, Iran. He is currently working on his Ph.D. thesis under the title of “Vibration analysis of smart functionally graded plates” at Smart Materials and Structures Lab in Faculty of Mechanical Engineering of the University of Tehran. His research interests include vibration analysis of plates and shells, smart materials and structures and functionally graded materials.